Collective excitations and their lineshapes for a compositional superlattice of type II

1997 J. Phys.: Condens. Matter 9 8041

(http://iopscience.iop.org/0953-8984/9/38/010)

J. Phys.: Condens. Matter **9** (1997) 8041–8054. Printed in the UK PII: S0953-8984(97)78606-5

Collective excitations and their lineshapes for a compositional superlattice of type II

A C Sharma†, R Sen†‡ and P Tripathi†

† Physics Department, Faculty of Science, MS University of Baroda, Vadodara 390 002, India
‡ School of Studies in Physics, Jiwaji University, Gwalior 474 011, India

Received 11 October 1996, in final form 4 April 1997

Abstract. The dielectric function and the density–density correlation function are calculated for a compositional superlattice of type II, which consists of alternate electron and hole layers (a two-component plasma) in an inhomogeneous dielectric background. The dielectric background of the electron gas is considered to be different from that of holes and the finite width of an electron (hole) layer is considered to allow both intrasubband and intersubband transitions. Our model superlattice consists of electron plasma, hole plasma, lattice vibrations of the background of the electron gas and lattice vibrations of the background of the hole gas. Electron–electron, electron–hole, hole–hole, electron–phonon, hole–phonon and phonon–phonon interactions take place in our model superlattice. Our calculation is applied to the $In_{1-x}Ga_xAs/GaSb_{1-y}As_y$ superlattice. Variation of plasmon–phonon coupled modes and their lineshapes with (x, y) and unit cell width has been investigated in order to study the effects of semiconductor to semimetal or vice versa phase transitions. It is found that phase transition prominently affects the plasmon modes, while phonon modes remain almost unaffected. The inhomogeneity in the background of the electron–hole gas also produces a significant change in plasma frequencies. Lineshapes of coupled plasmon–phonon modes for both semimetal and semiconductor phases are calculated and are computed with those of the homogeneous background. Significant changes in peak height and half width are observed due to inhomogeneity in the dielectric background and the semiconductor to semimetal phase transition.

1. Introduction

There has been immense interest in type-II superlattices because of an extraordinary band edge relationship at the interface and the co-existence of electron and hole gases [1–6]. The best known example of a type-II superlattice is $(InAs)_{1-x}(GaAs)_x/(GaSb)_{1-y}(GaAs)_y$. At the misaligned bandgap InAs/GaSb superlattice interface, electrons flood from the GaSb valence band to the InAs conduction band, leaving holes behind, and the process produces a dipole layer consisting of two-dimensional electron and hole gases. The calculated subband structure shows a strong dependence on the period of the superlattice (d) [7, 8]. The energy gap decreases with increasing d and the semiconductor to semimetal transition takes place at $d \cong 170$ Å. The electron concentration has been measured as a function of InAs layer thickness and a sudden increase of an order of magnitude has been observed for layer thickness $\cong 100$ Å [9]. Such an increase indicates the onset of electron transfer from GaSb to InAs. Far-infrared magneto-absorption experiments confirm a negative energy gap which suggests a semimetallic superlattice [10, 11]. The existence of a semiconductor to semimetal transition, which results in electron transfer from the GaSb layer to the InAs layer, when the InAs quantum well thickness reaches a threshold, was confirmed experimentally and

0953-8984/97/388041+14$19.50

theoretically [12, 13]. The electron mobility for InAs quantum well thickness from 150 to 200 Å ranges between 1.5 and 2.0×10^5 cm^2 V^{-1} s^{-1} at 4.2 K [14]. The conduction band minimum of InAs exists below the valence band maximum of GaSb, which yields the transfer of electrons from a GaSb layer to an InAs layer. The process results in a system where electrons and holes are mostly confined to adjacent layers. Therefore a type-II superlattice can be considered as a one-dimensional (1D) periodic array of electron and hole layers embedded in a dielectric medium which offers two different backgrounds for electrons and holes. The aim of this paper is to perform a theoretical study of electronic as well as ionic collective excitations and light scattering for a type-II superlattice, in order to see how the inhomogeneity in the background of the electron (hole) gas and the semiconductor to semimetal phase transition affect these properties. There have been a large number of experimental as well as theoretical studies on collective excitations and light scattering in semiconductor superlattices [5, 15–34], ever since the discovery of superlattices, because of their central importance in analysing and understanding several technological aspects of superlattices. The intrasubband plasma frequencies for a model type-II superlattice of 2D electron and hole layers has been calculated by Das Sarma and Quinn [32]. However, their work did not consider the finite width of an electron/hole layer and the inhomogeneity in the background. The work was then extended by Tselis and Quinn [17] by assigning finite width to electron (hole) layers in a homogeneous dielectric background. The theoretical study of intrasubband plasmons in a two-component system in a homogeneous background with the possibility of tunnelling between layers of zero width has also been performed [33]. Tzoar and Zhang [25] have performed a theoretical study on the Raman scattering cross section for a system of strictly 2D layers of electrons and holes in a homogeneous background. We present, in this paper, a calculation of plasmons and plasmon–phonon coupled modes and the line shapes of plasmon–phonon coupled modes for the $Ga_xIn_{1-x}As/GaAs_ySb_{1-y}$ superlattice. The superlattice has been modelled as a 1D sequence of electron (hole) layers which are embedded alternately in an inhomogeneous dielectric host medium. The lattice which consists of electrons is different from that containing holes, in a unit cell. Therefore, our model structure consists of four components, viz. electron plasma, hole plasma, phonons belonging to the lattice of $Ga_xIn_{1-y}As$ and the phonons of the $GaAs_ySb_{1-y}$ lattice. Also, we assign a finite width to an electron layer and a hole layer in order to take into account both intrasubband as well as intersubband plasmons. Our calculations incorporate electron–electron, hole–hole, electron–hole, electron–phonon, hole–phonon and phonon–phonon interactions for both intrasubband and intersubband transitions. Ours is a much more detailed and accurate calculation of plasmon–phonon modes and their line shapes for a type-II superlattice as compared with those reported in the past [17, 19, 25]. Further, we study the variation of plasma frequencies and their line shapes with (x, y) and with d, in order to see the changes in plasma frequencies for the semimetal to semiconductor or vice versa phase transition. The frequencies and line shapes have also been computed by considering a homogeneous background for the electron/hole gas to compare them with our calculated results. We present our calculations of collective excitations in section 2. The calculation and results on line shapes of coupled plasmon–phonon modes are given in section 3. We summarize our work in section 4.

2. Frequencies of collective excitations

The $In_{1-x}Ga_xAs/GaSb_{1-y}As_y$ superlattice consists of electrons in $In_{1-x}Ga_xAs$ layers and holes in $GaSb_{1-y}As_y$ layers. The superlattice offers a two-component plasma in an inhomogeneous background. The electron and hole plasmas interact with each other in

addition to their interaction with lattice vibrations of $In_{1-x}Ga_xAs$ and $GaSb_{1-y}As_y$. The frequencies of plasma oscillations and the plasmon-phonon coupled modes can be given by the zeros of the dielectric function of the system. A general expression for collective excitations in a type-II superlattice can be given by [33]

$$\begin{vmatrix} \epsilon_{11}^{\lambda} & \epsilon_{12}^{\lambda} \\ \epsilon_{21}^{\lambda} & \epsilon_{22}^{\lambda} \end{vmatrix} = 0. \tag{1}$$

The suffix 1 corresponds to the $In_{1-x}Ga_xAs$ layer while 2 corresponds to the $GaSb_{1-y}As_y$ layer of a unit cell. λ represents a composite subband index. The ϵ_{ii}^{λ} terms yield intralayer interactions, while ϵ_{ij}^{λ} terms give interlayer interactions. ϵ_{ij}^{λ} can be expressed as follows [34]:

$$\epsilon_{ij}^{\lambda} = \delta_{ij} - V_q P_{ii}^{\lambda}(q,\, \omega) T_{ij}^{\lambda}(q,\, k_z) \tag{2}$$

where T_{ij}^{λ} is the structure factor which takes care of periodic structure along the z-axis. P_{ii}^{λ} is the total polarizability (sum of electronic and ionic parts) of a layer and $V_q = 2\pi e^2/q$ is the 2D bare Coulomb interaction. We consider $\lambda = 0$ (intrasubband transitions) and $\lambda = 1$ (intersubband $0 \rightarrow 1$ transitions) for our calculation.

2.1. Intrasubband plasmons

The electronic part of polarizability involves both intrasubband and intersubband transitions. However, energies involved in intrasubband transitions are many times smaller than those involved in intersubband transitions. For example, energies involved in intrasubband transitions are smaller than 20 meV, whereas the intersubband energy gap between the ground subband and the first excited subband is of the order of 100 meV for the InAs layer. Therefore, the coupling between intrasubband plasmons and intersubband plasmons is weak and it can be neglected. After neglecting the coupling between intrasubband and intersubband transitions, (1) can be simplified for intrasubband plasmons:

$$\begin{aligned} |\epsilon^0(q,\, \omega,\, k_z)| = {} & \left\{1 + \alpha^0\left(P_{1e}^0 + P_{1i}\right)\right\}\left\{1 + \beta^0\left(P_{2h}^0 + P_{2i}\right)\right\} \\ & -\gamma^0\left(P_{2h}^0 + P_{2i}\right)\left(P_{1e}^0 + P_{1i}\right) = 0 \end{aligned} \tag{3}$$

where q and k_z are the components of wave vector along and perpendicular to an electron (hole) layer. The polarizabilities P_{1e}^0 and P_{2h}^0 are defined as

$$P_{1e}^0(q,\, \omega) = \frac{-n_{se}q^2}{\epsilon_{1\infty}m_1^*[\frac{1}{2}q^2v_{fe}^2 - \omega(\omega + \mathrm{i}\gamma_e)]} \tag{4}$$

$$P_{2h}^0(q,\, \omega) = -\frac{n_{sh}q^2}{\epsilon_{2\infty}m_2^*[\frac{1}{2}q^2v_{fh}^2 - \omega(\omega + \mathrm{i}\gamma_h)]}. \tag{5}$$

n_{se} and n_{sh} are the number of electrons and number of holes per unit area, respectively. v_{fe} (v_{fh}) and m_1^* (m_2^*) are Fermi velocity and the effective mass in layer one (two) of a unit cell, respectively. $\epsilon_{1\infty}$ and $\epsilon_{2\infty}$ are the optic dielectric constants of layers 1 and 2 of a unit cell. P_{1i} and P_{2i} are given by

$$P_{1i}(q,\, \omega) = \frac{-q^2(\omega_{L1}^2 - \omega_{T1}^2)}{(\omega_{T1}^2 - \omega(\omega + \mathrm{i}\gamma_{ph}))}\left(\frac{d_1}{4\pi e^2}\right) \tag{6}$$

$$P_{2i}(q,\, \omega) = \frac{-q^2(\omega_{L2}^2 - \omega_{T2}^2)}{(\omega_{T2}^2 - \omega(\omega + \mathrm{i}\gamma_{ph}))}\left(\frac{d_2}{4\pi e^2}\right) \tag{7}$$

where d_1 and d_2 are thicknesses of layers 1 and 2 of a unit cell. ω_{L2} (ω_{L2}) and ω_{T1} (ω_{T2}) are the longitudinal and transverse optical phonon frequencies of a $In_{1-x}Ga_xAs$ ($GaSb_{1-y}As_y$) layer, respectively. γ_e, γ_h and γ_{ph} are the damping constants for the electron plasma, hole plasma and phonons, respectively. For calculation of coupled modes of plasmons and phonons, we take $\gamma_e = \gamma_h = \gamma_{ph} = 0$. $\alpha^0(q, k_z)$, $\beta^0(q, k_z)$ and $\gamma^0(p, k_z)$ are defined as follows:

$$\alpha^0(q, k_z) = -\left(\frac{2\pi e^2}{q}\right)\left\{H_{11}^0(q) - F_{11}^0(q)\left[1 - S(q, k_z)\right]\right\} \tag{8}$$

$$\beta^0(q, k_z) = -\left(\frac{2\pi e^2}{q}\right)\left\{H_{22}^0(q) - F_{22}^0(q)\left[1 - S(q, k_z)\right]\right\} \tag{9}$$

$$\gamma^0(q, k_z) = \left(\frac{2\pi e^2}{q}\right)^2 F_{12}^0(q)F_{21}^0(q)\left[R(q, k_z) + S^2(q, k_z)\right] \tag{10}$$

where matrix element $H_{ij}^{\lambda}(q)$ is defined as

$$H_{ij}^{\lambda}(q) = \int_{-d_i/2}^{d_i/2} \mathrm{d}t \int_{-d_j/2}^{d_j/2} \mathrm{d}t' \mathrm{e}^{-q|t-t'|}\psi_i^{\lambda}(t')\psi_i^{\lambda}(t) \tag{11}$$

t and t' vary over the width of an electron (hole) layer. $F_{ij}^{\lambda}(q)$ is given by (11) on replacing $q|t' - t'|$ by $q(t - t')$. $H_{ij}^{\lambda}(q)$ and $F_{ij}^{\lambda}(q)$ have been calculated using infinite potential well wave functions as the envelope functions for both electron and hole layers in a unit cell. It is to be mentioned that an infinitely deep potential well model does not properly take into account certain effects such as those arising from charge transfer. However, it can be used to calculate matrix elements $H_{ij}^{\lambda}(q)$ and $F_{ij}^{\lambda}(q)$ because the matrix elements are not so sensitive to the choice of single-particle potential. The explicit values of $H_{ij}^{\lambda}(q)$ and $F_{ij}^{\lambda}(q)$ are given in [34]. $S(q, k_z)$ and $R(q, k_z)$ are defined by

$$S(q, k_z) = \frac{\sinh(qd)}{\cosh(qd) - \cos(k_z d)} \tag{12a}$$

$$R(q, k_z) = \frac{1 - \cosh(qd)}{\cosh(qd) - \cos(k_z d)}. \tag{12b}$$

Equation (3) has two terms on the right-hand side. Two brackets in the first term contain the intralayer dielectric functions for $Ga_{1-x}In_xAs$ and $GaSb_{1-y}As_y$ layers, respectively, of a unit cell, while the second term yields the interlayer interaction between the collective excitations in two layers of a unit cell. The effects of electron–electron interaction and hole–hole interaction appear through $\alpha^0 P_{1e}^0$ and $\beta^0 P_{2h}^0$, respectively. $(\alpha^0\beta^0 - \gamma^0)P_{1e}^0 P_{2h}^0$ consists of electron–hole interactions, for intrasubband transitions. $\alpha^0(P_{1e}^0 + P_{1i})$ and $\beta^0(P_{2h}^0 + P_{2i})$ contain plasmon–phonon coupling, while $(\alpha^0\beta^0 - \gamma^0)P_{1e}^0 P_{2h}^0$ and $(\alpha^0\beta^0 - \gamma^0)P_{1i}P_{2i}$ involve plasmon–plasmon and phonon–phonon couplings, respectively. On substituting (4)–(7), (3) become a fourth-order equation in ω^2 and it has four roots which involve plasmon–phonon, plasmon–plasmon and phonon–phonon coupling. The intralayer coupling yields two coupled plasmon–phonon modes in each layer. We represent these four coupled modes by L_1–L_4. In order to see separately the effect of plasmon–plasmon couplings in a simple manner, we take $\omega \to 0$ limits of (6) and (7) to solve (3) for small q at $k_z d \to 0$ and $k_z d \to \pi$. $k_z d \to 0$ refers to the case of strong coupling among the layers, while $k_z d \to \pi$ refers to the case of weak coupling among the layers. We obtain two roots of (3), which yield frequencies of two coupled plasmon–plasmon modes.

$$\omega_P^+(q, 0) = \left[4\pi e^2\left\{\frac{n_{se}}{\epsilon_{1\infty}m_1^*} + \frac{n_{sh}}{\epsilon_{2\infty}m_2^*}\right\}\Big/\left\{\frac{\epsilon_{10}}{\epsilon_{2\infty}}d_1 + \frac{\epsilon_{20}}{\epsilon_{2\infty}}d_2\right\}\right]^{1/2} \tag{13a}$$

$$\omega_P^+(q,\ \pi/d) = \left\{\frac{2\pi e^2 n_{se} d}{m_1^* \epsilon_{1\infty}}\right\}^{1/2} q \tag{13b}$$

$$\omega_P^-(q,\ 0) \quad = \left[\left(\frac{2\pi e^2 n_{sh} d}{\epsilon_{2\infty} m_2^*}\right) \Big/ \left(1 + \frac{n_{sh} m_1^* \epsilon_{1\infty}}{n_{se} m_2^* \epsilon_{2\infty}}\right)\right]^{1/2} q \tag{13c}$$

$$\omega_P^-(q,\ \pi/d) = \left(\frac{2\pi e^2 n_{sh} d}{m_2^* \epsilon_{2\infty}}\right)^{1/2} q \tag{13d}$$

where $\epsilon_{1\infty}$ and $\epsilon_{2\infty}$ are static dielectric constants of $Ga_xIn_{1-x}As$ and $GaSb_{1-y}As_y$, respectively. The plasmon–plasmon coupling provides a full band (ω_P^-) for 2D acoustic plasmons. It is obvious from (13*a*)–(13*d*) that $\omega_P^{\pm}(q,\ 0)$ depend on the intrinsic parameters of both the layers of a unit cell, while $\omega_P^+(q,\ \pi/d)$ and $\omega_P^-(q,\ \pi/d)$ depend on the intrinsic parameters of $Ga_xIn_{1-x}As$ and $GaSb_{1-x}As_y$, respectively. However, both $\omega_P^{\pm}(q,\ k_z)$ depend on $(x,\ y)$ and d. $\omega^+(q,\ \pi/d)$, $\omega_P^-(q,\ 0)$ and $\omega_P^-(q,\ \pi/d)$ exhibit $d^{1/2}$-dependence, while $\omega_P^+(q,\ 0)$ shows $d^{-1/2}$-dependence. The $(x,\ y)$-dependence has been taken into account through $\epsilon_{1\infty}$, $\epsilon_{2\infty}$, m_1^* and m_2^* in the following simple manner:

$$\epsilon_{1\infty} = (1-x)\epsilon_\infty(\text{InAs}) + x\epsilon_\infty(\text{GaAs}) \tag{14a}$$

$$\epsilon_{2\infty} = (1-y)\epsilon_\infty(\text{GaSb}) + y\epsilon_\infty(\text{GaAs}) \tag{14b}$$

$$m_1^* = (1-x)m_e^*(\text{InAs}) + xm_e^*(\text{GaAs}) \tag{15a}$$

$$m_2^* = (1-y)m_h^*(\text{GaSb}) + ym_h^*(\text{GaAs}) \tag{15b}$$

ω_{L1} (ω_{L2}) and ω_{T1} (ω_{T2}) also depend weakly on $(x,\ y)$. We however treat them as independent of $(x,\ y)$ in our calculation. It has to be mentioned that (14) and (15) are valid for small values of x and y.

We computed L_1–L_4 coupled modes by modelling the $Ga_xIn_{1-x}As/GaSb_{1-y}As_y$ superlattice in terms of the following values of parameters [35–39]: $\epsilon_\infty(\text{InAs}) = 12.3$, $\epsilon_\infty(\text{GaSb}) = 14.4$, $\epsilon_\infty(\text{GaAs}) = 10.9$, $m_e^*(\text{InAs}) = 0.026m_e$, $m_h^*(\text{GaSb}) = 0.3m_e$, $m_e^*(\text{GaAs}) = 0.07m_e$, $m_h^*(\text{GaAs}) = 0.7m_e$, $\omega_{T1} = 26.91$ meV, $\omega_{L1} = 29.53$ meV, $\omega_{T2} = 28.22$ meV, $\omega_{L2} = 30.14$ meV, $n_{Se} \equiv n_{Sh} = 7 \times 10^{11}$ cm^{-2}. It has to be mentioned that the $Ga_xIn_{1-x}As/GaAs_ySb_{1-y}$ superlattice exhibits semimetal properties for $(x,\ y) \leqslant 0.25$ and it exhibits semiconductor properties for $(x,\ y) \geqslant 0.25$. Further, the transition from semiconductor to semimetal phase also takes place on changing d. For example the InAs/GaSb ($x = y = 0$) superlattice transforms from semimetal to semiconductor phase for $d \leqslant 170$ Å. Therefore, the transition from semiconductor to semimetal phase or vice versa can be studied in our calculations by varying both $(x,\ y)$ and d. Our computed results show that the change in L_3 and L_4 on changing both $(x,\ y)$ and d is almost negligible. However, L_1 and L_2 exhibit a significant change with $(x,\ y)$ and with d. It is found that for changing $x = y$ from 0 to 0.5 and keeping $d = 420$ Å and $q = 1.31 \times 10^5$ cm^{-1}, L_1 roughly reduces by 17%, whereas L_2 reduces by 23% for all values of $\cos(k_z d)$. $\omega_P^+(q,\ k_z)$ and $\omega_P^-(q,\ k_z)$ are plotted as function of $x = y$ in figure 1 for $qd_1 = 0.265$, $qd_2 = 0.2882$ and $k_z d = 3.9513$. Both x and y are varied from 0 to 0.5. At higher values of x and y, the validity of (14) and (15) may become questionable and also the type-II nature of $Ga_xIn_{1-x}As/GaSb_{1-y}As_y$ may not hold. The figure shows that $\omega_P^{\pm}(q,\ k_z)$ decreases on increasing x and they are almost proportional to $1/\sqrt{x}$. $\omega_P^-(q,\ k_z)$ is much softer than $\omega_P^+(q,\ k_z)$. The effect of semiconductor to semimetal phase transition (in terms of variation of d) on $\omega_P^{\pm}(q,\ k_z)$ at fixed values of x and y can be understood from (13*a*)–(13*d*). Further, on computing $\omega_P^{\pm}(q,\ k_z)$ as a function of d for $x = y = 0$, $q = 1.31 \times 10^5$ cm^{-1} and $k_z = 9.357 \times 10^5$ cm^{-1} [35], we find that $\omega_P^+(q,\ 0)$ decreases

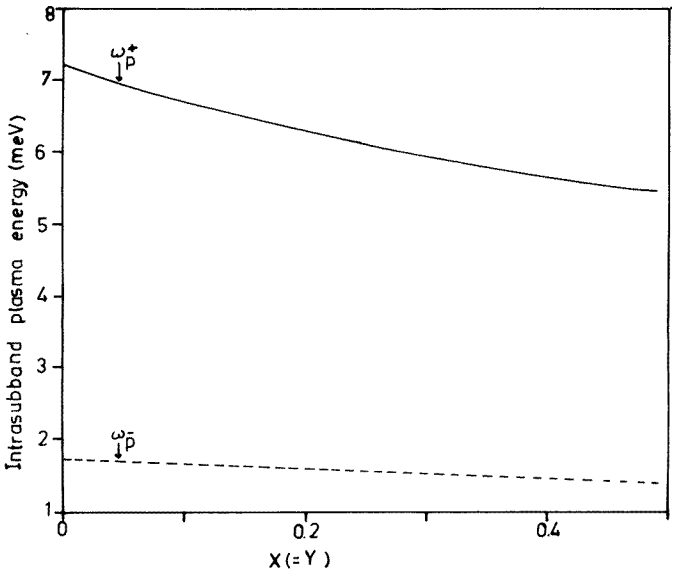

Figure 1. Intrasubband electron and hole plasmon frequencies, $\omega_P^+(q, k_z)$ (solid curve) and $\omega_P^-(q, k_z)$ (dashed curve) plotted as functions of (x, y) at $q = 1.31 \times 10^5$ cm^{-1}, $k_z = 9.357 \times 10^5$ cm^{-1} and $d = 420$ Å.

as $1/\sqrt{d}$, while $\omega_P^-(q, 0)$ increases as $\sqrt{d}$, on increasing d, which is supported by (13). It should be mentioned that the values of plasma frequencies are larger for the semiconductor phase and are smaller for the semimetal phase of a type-II superlattice.

Our computed L_1–L_4 are plotted in figure 2 as functions of qd at $x = y = 0$, $d_1 = 200$ Å and $d_2 = 220$ Å for $-1 \leqslant \cos(k_z d) \leqslant 1$. The values of other parameters are taken to be the same as those used above. The figure shows that L_1 and L_2 form bands of 2D plasmons. The band of L_2 is wider than that of L_1. All the plasmon modes of L_1 go to zero as linear functions of q, while in the case of band L_2 the plasmon modes which are linear in q and tend to zero as $q \to 0$ appear for $\cos(k_z d)$ not close to unity. The other modes go to a constant value as $q \to 0$. The figure also shows that the plasmons of L_1 and L_2 bands increase on increasing qd. This suggests that, at a fixed d-value, plasma frequency increases on increasing q.

We have also studied the effect of inhomogeneity in the dielectric background by calculating ω_P^- and ω_P^+ for a homogeneous dielectric background of an electron (hole) gas. It is noticed that the effect of inhomogeneity in the dielectric background is more prominent in the ω_P^- band, while it is less significant in the ω_P^+ band. The effect of inhomogeneity increases the value of ω_P^+ and it decreases the value of ω_P^-, as can also be seen from (13*a*)–(13*d*).

The solution of (3) with the use of the $\omega \to 0$ limit of (4) and (5) yields two values of ω (ω_{Ph}^+ and ω_{Ph}^-) which are coupled phonon–phonon modes. The computation of ω_{Ph}^- and ω_{Ph}^+ exhibits a weak q-dependence, for all possible values of $\cos(k_z d)$. Also, ω_{Ph}^- and ω_{Ph}^+ do not show any significant change on varying x and y in the range of 0–0.5. This suggests that phonon frequencies are more or less unaffected during semiconductor to semimetal or vice versa phase transition. Our results show that the computed values of ω_P^+, ω_P^-, ω_{Ph}^+ and ω_{Ph}^- are approximately equal to those of L_1–L_4, respectively. We further noticed that the computed values of ω_{Ph}^- and ω_{Ph}^+ significantly differ from the values of

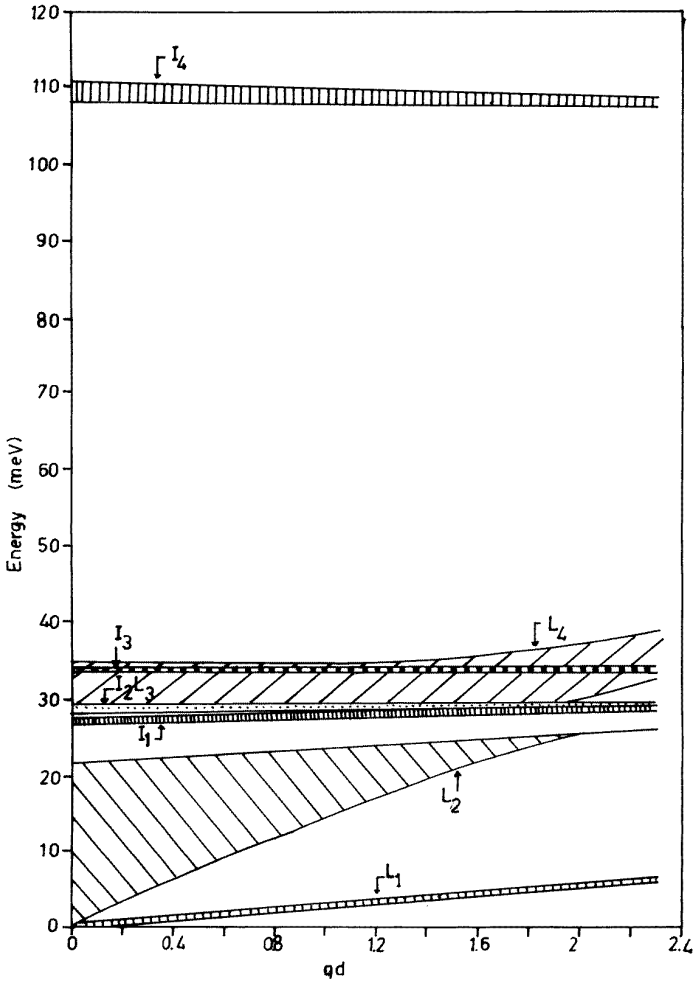

Figure 2. The coupled intrasubband plasmon–phonon modes (L_1–L_4) and the coupled intersubband plasmon–phonon modes (I_1–I_4) are plotted as functions of qd, for $d = 420$ Å and $x = y = 0$. The upper bound of L_2–L_4, I_1 and I_2 belongs to $\cos(k_z d) = 1$, whereas the lower bound of I_1 and I_4 belongs to $\cos(k_z d) = 1$.

bulk phonon frequencies ω_{L1} and ω_{L2}, respectively. We find that $\omega_{T1} < \omega_{Ph}^{-} < \omega_{L1}$ and $\omega_{T2} < \omega_{Ph}^{+} < \omega_{L2}$. This suggests that ω_{Ph}^{+} and ω_{Ph}^{-} represent the interface phonon frequencies which are produced by the coupling between lattice vibrations of two adjoint layers of different dielectric constants, in our model superlattice. Our findings are supported by experimental measurement of phonon frequencies in InAs/GaSb superlattice [37]. L_3 and L_4 are also plotted as functions of q in figure 2.

2.2. Intersubband plasmons

After neglecting the coupling between intrasubband and intersubband transitions, (1) takes the following form for intersubband plasmons ($\lambda = 1$):

$$\left|\epsilon^1(q,\,\omega,\,k_z)\right| = 1 + \alpha^1 P_{1e}^1 + \alpha^0 P_{1i} + \beta^1 P_{2h}^1 + \beta^0 P_{2i} + \alpha^1\beta^1 P_{1e}^1 P_{2h}^1 + \alpha^0\beta^1 P_{1i} P_{2h}^1$$

$$+\alpha^1\beta^0 P^1_{1e}P_{2i} + \alpha^0\beta^0 P_{1i}P_{2i} - \gamma^1\Big(P^1_{2h}P^1_{1e} + P^1_{2h}P_{1i} + P_{2i}P^1_{1e}\Big) - \gamma^0 P_{2i}P_{1i} \tag{16}$$

where $\alpha^1(q,\, k_z)$, $\beta^1(q,\, k_z)$ and $\gamma^1(q,\, k_z)$ are defined as

$$\alpha^1\big(q,\, k_z\big) = -\left(\frac{2\pi e^2}{q}\right)\Big\{H^1_{11}(q) - F^1_{11}(q)\big[1 - S\big(q,\, k_z\big)\big]\Big\} \tag{17}$$

$$\beta^1\big(q,\, k_z\big) = -\left(\frac{2\pi e^2}{q}\right)\Big\{H^1_{22}(q) - F^1_{22}(q)\big[1 - S\big(q,\, k_z\big)\big]\Big\} \tag{18}$$

$$\gamma^1\big(q,\, k_z\big) = \left(\frac{2\pi e^2}{q}\right)^2 F^1_{12}(q)F^1_{21}(q)\Big[R\big(q,\, k_z\big) + S^2\big(q,\, k_z\big)\Big]. \tag{19}$$

The explicit values of the matrix elements H^1_{11}, H^1_{22}, F^1_{11}, F^1_{22}, F^1_{12} and F^1_{21} are defined by (11) and these are evaluated in [34]. P^1_{1e} and P^1_{2h} are given by

$$P^1_{1e} = -\frac{2n_{se}E_{10e}}{\epsilon_{1\infty}[E^2_{10e} - \omega(\omega + \mathrm{i}\gamma_e)]} \tag{20}$$

$$P^1_{2h} = \frac{-2n_{sh}E_{10h}}{\epsilon_{1\infty}[E^2_{10h} - \omega(\omega + \mathrm{i}\gamma_h)]}. \tag{21}$$

S, R, P_{1i} and P_{2i} are defined earlier by (12*a*), (12*b*), (6) and (7), respectively. E_{10e} and E_{10h} are the energy band gaps between the ground subband and the first subband for electrons and holes, respectively. E_{10e} and E_{10h} can be calculated using an infinitely deep potential well model for the electron and hole layers. We however found that the computed values of E_{10e} using the infinitely deep potential well model show a large discrepancy in comparison with experimentally measured values as a function of d_1 [35]. This suggests that the calculated $E_{10e/h}$ using an infinitely deep potential well model require modifications to incorporate important effects, such as those arising from charge transfer in the self-consistent single-particle potential. To remain simple, we modified the calculated $E_{10e/h}$ to the following empirical relation which fits well the experimentally measured values of $E_{10e/h}$:

$$E_{10e/h} = \frac{A_{e/h}}{d_{e/h}} + \frac{B_{e/h}}{d^2_{e/h}}. \tag{22}$$

We estimate $A_e = 17.7514\times10^3$ meV Å^{-1}, $B_e = 436.1082\times10^3$ meV Å^{-2}, $A_h = 5.2258\times10^3$ meV Å^{-1} and $B_h = 37.796\times10^3$ meV Å^{-2} to fit the experimentally measured values of E_{10e} and E_{10h} [35]. Similar to the case of (3), we notice that (16) involves plasmon–plasmon, plasmon–phonon and phonon–phonon interactions. Equation (16) consists of coupling among intersubband electron and hole plasmons, and the lattice vibrations of $In_{1-x}Ga_xAs$ and $GaAs_ySb_{1-y}$ layers. The computed four roots of (16) are also plotted as functions of q in figure 2. The coupled intersubband plasmon–phonon modes are represented by I_1–I_4. We notice from figure 2 that the bands of I_1, I_2, L_3 and L_4 (which correspond to phonon frequencies) overlap each other. The band of I_3 overlaps the band of L_4 for our choice of the values of parameters. I_3 and I_4 approximately represent coupled plasmon–plasmon modes for intersubband transitions, while I_1 and I_2 approximately represent the interface phonon modes. The plasmon–plasmon coupled modes (ω_1 and ω_2) for intersubband transitions are given by the roots of (16) on taking static limit of P_{1i} and P_{2i}, while phonon–phonon coupled modes (ω_3 and ω_4) are given by the two roots of (16) on substituting static limits of P^1_{1e} and P^1_{2h}. It is to be noted here that ω_3 and ω_4 slightly differ from ω^-_{Ph} and ω^+_{Ph} because of the different nature of electron (hole) transitions involved in the two cases. We

compute ω_1–ω_4 as functions of d for $q = 1.31 \times 10^5$ cm^{-1}, $k_z = 9.357 \times 10^5$ cm^{-1} and $x = y = 0$. ω_1 and ω_2 show a strong d-dependence, while ω_3 and ω_4 weakly depend on d. ω_1 and ω_2 are plotted as functions of d in figure 3, for 100 Å$\leqslant d \leqslant$ 800 Å. For very small values of d (<100 Å or so) tunnelling between the layers, which is not considered in this paper, may become important and significantly change our results. Similarly, for very large values of d (>800 Å or so) the modelling of an electron (hole) layer as a infinite potential well may not be properly justified. The figure shows that ω_1 and ω_2 decrease on increasing d. ω_1 exhibits relatively stronger d-dependence than ω_2. The figure shows that ω_1 and ω_2 decrease rather rapidly for 100 Å$\leqslant d \leqslant$ 600 Å at given values of q, k_z and (x, y). It can be seen from the figure that for larger values of d_1 and d_2 intersubband plasma frequencies reduce drastically and they even become comparable with intrasubband plasma frequencies. Our computed values of ω_1 show very good agreement with experimentally measured values of ω_1 for different values of d_1 [35]. The reported experimental values of ω_1 are for the InAs/AlSb superlattice, whereas our computed ω_1-values are for the InAs/GaSb superlattice. The experimental values of ω_1 vary in the range of 160–125 meV, whereas our computed values vary from 146 to 111 meV, for 150 Å$\leqslant d_1 \leqslant$ 200 Å at $q = 1.31 \times 10^5$ cm^{-1} and $k_z = 9.357 \times 10^5$ cm^{-1}.

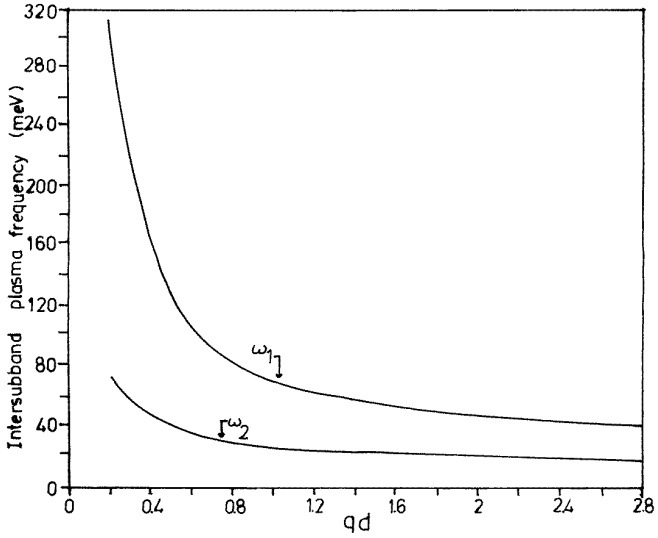

Figure 3. Intersubband plasma frequencies (ω_1 and ω_2) are plotted as functions of d for $q = 1.31 \times 10^5$ cm^{-1}, $k_z = 9.357 \times 10^5$ cm^{-1}.

3. The line shapes of plasmon–phonon coupled modes

The lineshapes can be given by the imaginary part of dynamical polarizability $\chi(q, \omega, z, z')$ which can be obtained by solving the integral equation [24]

$$\chi(q, \omega, z, z') = P(q, \omega, z, z') + \int\int \mathrm{d}_{z_1}\,\mathrm{d}_{z_2} V(q, \omega, z_1, z_2)\chi(q, \omega, z_2, z') \tag{23}$$

where $P(q,\ \omega,\ z,\ z')$ is the polarizability in the absence of Coulomb electron–electron interaction, V, which is given as

$$V(q,\ z,\ z') = \left(\frac{2\pi e^2}{q}\right)\exp(-q|z - z'|). \tag{24a}$$

For our model superlattice structure of type II, z can be taken as follows:

$$z = Id + R_i + t \tag{24b}$$

where I is the unit cell index whereas i is the layer index within a unit cell. Each unit cell consists of two layers which are represented by two values of i. The confinement of electrons (holes) in a layer generates the subband structure. Both intrasubband and intersubband transitions are possible between different subbands. For intrasubband transitions in the ground subband and intersubband transition between the ground subband and the first excited subband, we obtain [24, 34]

$$\chi^{\lambda}_{ij}(q,\ \omega,\ I,\ I',\ t,\ t') = P^{\lambda}_{ij}(q,\ \omega,\ t,\ t')\delta_{II'}\delta_{ij} + \sum_{I_1}\sum_{j'}\int\int \mathrm{d}t_1\,\mathrm{d}t_2 V_{ij}\big(q,\ I,\ I_1,\ t,\ t_1\big)$$
$$P^{\lambda}_{ii}\big(q,\ \omega,\ t_1,\ t_2'\big)\chi^{\lambda}_{j'j}\big(q,\ \omega,\ I_1,\ I',\ t_2,\ t'\big) \tag{25}$$

with

$$V_{ij}(q,\ I,\ I',\ t,\ t') = \left(\frac{2\pi e^2}{q}\right)\exp\big(-q|(I - I')d + R_{ij} + (t - t')|\big) \tag{26}$$

where $R_{ij} = R_i - R_j$ and P^{λ}_{ii} is the total (electronic and ionic) polarizability of the ith layer. The lineshapes of different coupled plasmon–phonon modes are given by [34]

$$L\big(q,\ k_z,\ \omega\big) = -\mathrm{Im}\Big[\chi^0_{11}\big(q,\ \omega,\ k_z\big) + \chi^0_{12}\big(q,\ \omega,\ k_z\big) + \chi^0_{21}\big(q,\ \omega,\ k_z\big) + \chi^0_{22}\big(q,\ \omega,\ k_z\big)$$
$$+\chi^1_{11}\big(q,\ \omega,\ k_z\big) + \chi^1_{12}\big(q,\ \omega,\ k_z\big) + \chi^1_{21}\big(q,\ \omega,\ k_z\big) + \chi^1_2\big(q,\ \omega,\ k_z\big)\Big] \tag{27}$$

where $\chi^{\lambda}_{ij}(q,\ k_z)$ are obtained by Fourier transforming (25) with respect to the layer index. Each term on the right-hand side of (27) is simplified in terms of P^0_{1e}, P^0_{2h}, P^1_{1e}, P^1_{2h}, P_{1i} and P_{2i}. We obtain

$$\chi^0_{11} = \frac{1}{|\epsilon^0|}\Big[-\Big(P^0_{1e} + P_{1i}\Big)\Big(1 - v_q\Big(P^0_{2h} + P^0_{2i}\Big)L^0_{22}\Big)A^0_{11}\Big] \tag{28}$$

$$\chi^1_{11} = \frac{1}{|\epsilon^0|}\Big[-\Big(P^1_{1e} + P_{1i}\Big)\Big(1 - v_q\Big(P^1_{2h} + P_{2i}\Big)L^1_{22}\Big)A^1_{11}\Big] \tag{29}$$

$$\chi^0_{12} = \frac{1}{|\epsilon^0|}\Big[-v_q\Big(P^0_{1e} + P_{1i}\Big)F^0_{12}w_{12}\Big(P^0_{2h} + P_{2i}\Big)A^0_{12}\Big] \tag{30}$$

$$\chi^1_{12} = \frac{1}{|\epsilon^1|}\Big[-v_q\Big(P^1_{1e} + P_{1i}\Big)F^1_{12}w_{12}\Big(P^1_{2h} + P_{2i}\Big)A^1_{12}\Big] \tag{31}$$

$$\chi^0_{12} = \frac{1}{|\epsilon^0|}\Big[-v_q\Big(P^0_{2h} + P_{2i}\Big)F^0_{21}w_{21}\Big(P^0_{1e} + P_{1i}\Big)A^0_{21}\Big] \tag{32}$$

$$\chi^1_{21} = \frac{1}{|\epsilon^1|}\Big[-v_q\Big(P^1_{2h} + P_{2i}\Big)F^1_{21}w_{21}\Big(P^1_{1e} + P_{1i}\Big)A^1_{21}\Big] \tag{33}$$

$$\chi^0_{22} = \frac{1}{|\epsilon^0|}\Big[-\Big(P^0_{2h} + P_{2i}\Big)\Big(1 - v_q\Big(P^0_{1e} + P_{1i}\Big)L^0_{11}\Big)A^0_{22}\Big] \tag{34}$$

$$\chi^1_{22} = \frac{1}{|\epsilon^1|}\Big[-\Big(P^1_{2h} + P_{2i}\Big)\Big(1 - v_q\Big(P^1_{1e} + P_{1i}\Big)L^1_{11}\Big)A^1_{22}\Big] \tag{35}$$

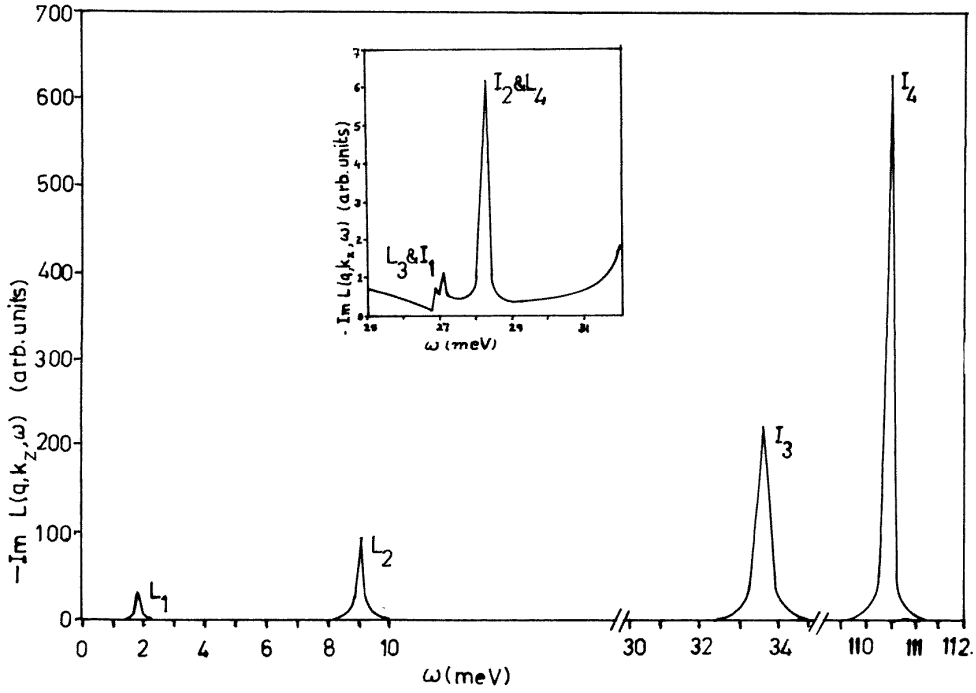

Figure 4. A plot of $-\mathrm{Im}\,L(q,\,\omega,\,k_z)$ as a function of ω for $d = 420$ Å, $k_z = 9.357 \times 10^5$ cm^{-1} and $q = 1.31 \times 10^5$ cm^{-1}.

with

$$A_{ij}^{\lambda} \equiv A_{ij}^{nm} = |\langle n|\exp(-\mathrm{i}k_z t)|m\rangle|^2 \tag{36}$$

where A_{ij}^{λ} can be obtained from F_{ij}^{λ} on replacing (qd_i) by $\mathrm{i}k_z d_i$. L_{ij}^{λ} are defined as

$$L_{ij}^{\lambda} = H_{ij}^{\lambda} - F_{ij}^{\lambda}\left[1 - w_{ij}(q,\,k_z)\right] \tag{37}$$

where

$$w_{ij}(q,\,k_z) = \left[\frac{\exp(-q|R_{ij}|)\,\exp(\mathrm{i}k_z d)}{\exp(\mathrm{i}k_z d) - \exp(-qd)} + \frac{\exp(q|R_{ij}|)\,\exp(-qd)}{\exp(-\mathrm{i}k_z d) - \exp(-qd)}\right]. \tag{38}$$

P_{1e}^0, P_{1e}^1, P_{2h}^0, P_{2h}^1, P_{1i} and P_{2i} have been defined earlier.

Equation (27) describes the lineshapes for different coupled plasmon–phonon modes, which appear in the scattered light spectrum of a superlattice of type II. The peak positions of these lineshapes represent the frequencies of different coupled plasmon–phonon modes originating from the interaction between intrasubband plasmons, intersubband plasmons and the phonons. As is obvious from (27), our calculated values of $L(q,\,\omega,\,k_z)$ consists of four components of polarizability, viz. χ_{11}^{λ}, χ_{12}^{λ}, χ_{21}^{λ} and χ_{22}^{λ}, each of which has two components. We have computed $L(q,\,\omega,\,k_z)$ as a function of ω using $q = 1.31 \times 10^5$ cm^{-1}, $k_z = 9.357 \times 10^5$ cm^{-1}, $\gamma_e = 0.2$, $\gamma_h \equiv \gamma_{ph} = 0.1$ meV for two values of d, i.e. $d = 160$ Å (semiconductor phase) and $d = 420$ Å (semimetal phase) at different values of $(x,\,y)$. The values of other parameters have been taken as the same as used previously. Our computed $-\mathrm{Im}\,L(q,\,\omega,\,k_z)$ for $x = y = 0$ and $d = 420$ Å are plotted in figure 4. The figure demonstrates that the lineshapes of L_1, I_3, L_2, I_4, L_4 and L_3 are well resolved. The

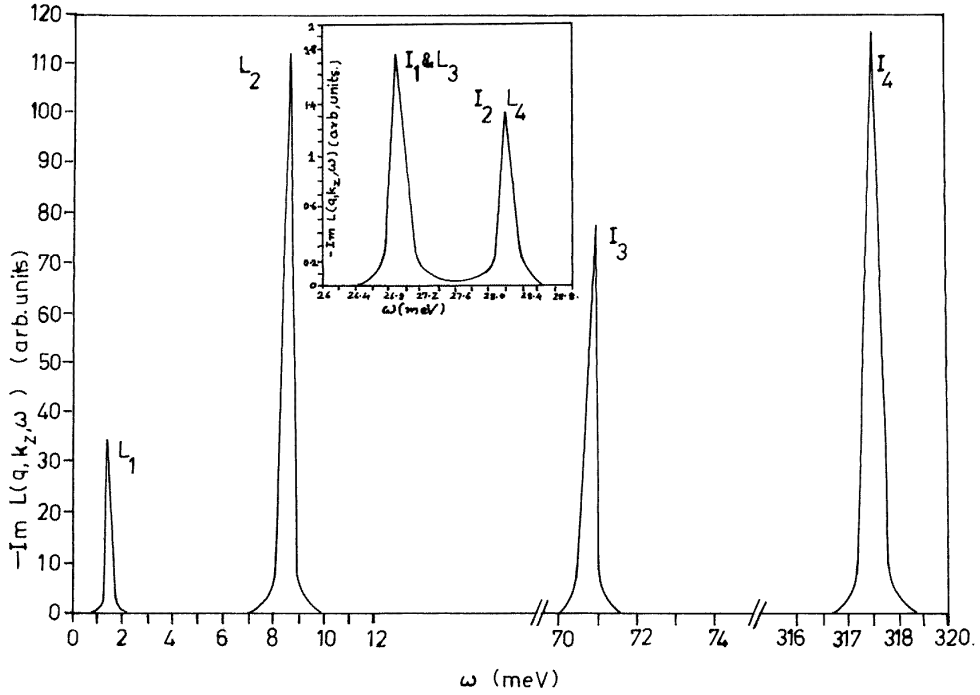

Figure 5. A plot of $-\mathrm{Im}\,L(q,\,\omega,\,k_z)$ as a function of ω for $d = 160$ Å, $k_z = 9.357 \times 10^5$ cm^{-1} and $q = 1.31 \times 10^5$ cm^{-1}.

lineshapes of I_1 and I_2 overlap with those of L_3 and L_4. The lineshapes at L_1, I_3, L_2 and I_4 have relatively larger peak height, whereas lineshapes of L_4 and L_3 have a small peak height. The lineshapes of L_3 and L_4 are shown in the inset for clarity. All these lineshapes could be observed in the light scattering experiments. Lineshapes of coupled plasmon–phonon modes obtained for the semimetal phase are also calculated for homogeneous background to compare our calculation for inhomogeneous background. No significant change due to inhomogeneity in the background is observed.

The lineshapes for the semiconductor phase of a type-II superlattice ($x = y = 0$ and $d = 160$ Å) are shown in figure 5. On comparing figures 4 and 5, we notice the following: (i) there is an insignificant change in the peak positions and peak heights of L_3, I_1, L_4 and I_2 modes on changing d from 420 Å to 160 Å. (ii) The positions of L_1 and L_2 are shifted towards lower energy values, while the positions of I_3 and I_4 modes are shifted to the higher energy-side on decreasing d. (iii) The peak heights of L_1 and L_2 show a small change, while the peak heights of I_3 and I_4 have been reduced drastically on decreasing the value of d from 420 to 160 Å. Our computed lineshapes of L_3 and L_4 qualitatively agree with the experimentally measured phonon lineshape in the InAs/GaSb superlattice [37]. Also, our computed lineshape of I_4 shows good qualitative agreement with the experimentally measured lineshape of the intersubband electron plasma in the InAs/AlSb superlattice [35].

4. Conclusion

We have performed a model calculation of the dielectric function and density–density correlation function for a compositional type-II $Ga_xIn_{1-x}As/GaAs_ySb_{1-y}$ superlattice by taking into account the difference in dielectric background of electron and hole gas and the finite width of an electron (hole) layer. Our calculation consists of 12 possible interaction terms and it is a more accurate analysis than those performed in the past. $\omega_P^{\pm}$, ω_1 and ω_2 exhibit a strong dependence on (x, y), d and the inhomogeneity in the dielectric background, whereas $\omega_{ph}^{\pm}$, ω_3 and ω_4 show insignificant change on varying (x, y) and d. Our computed $\omega_{ph}^{\pm}$, ω_3 and ω_4 are closer to interface phonon modes than LO bulk phonon modes. ω_P^{+} and ω_1^0 depend on the intrinsic parameters of both layers in a unit cell, whereas ω_P^{-} and ω_2 depend on the intrinsic parameters of $GaSb_{1-y}As_y$ only. The lineshapes of L_1, L_2, I_3, I_4, L_4 and L_3 are well resolved. The lineshapes of I_1 and I_2 overlap with those of L_4 and L_3. Also, the lineshapes of L_1, I_3, L_2 and I_4 have a reasonably large peak height and half width which can be measured experimentally. The lineshapes of L_3, I_1, L_4 and I_2 show insignificant change on changing d, while the positions of L_1 and L_2 shift towards lower energy and the positions of I_3 and I_4 shift towards the higher-energy side on decreasing d. The peak heights of L_1 and L_2 show a small change, while the peak heights of I_3 and I_4 reduce drastically on decreasing d from 420 to 160 Å.

Acknowledgments

ACS and PT acknowledge financial support from the Department of Science and Technology, New Delhi. RS thanks MS University for providing research facilities in the Physics Department and for hospitality during her stay in Baroda.

References

[1] Wang P L and Xiong S J 1994 *Phys. Rev.* B **49** 10 373–80
[2] Bresler M S, Gusev O B, Titkov A N, Cheban V N, Yakovlev Y P, Hulicius E, Oswald J, Pangrac J and Simecek J 1993 *Semiconductor* **27** 341–8
[3] De-paula A M and Weber G 1994 *Appl. Phys. Lett.* **65** 1281–3
[4] Nicholas R J, Burgt M V, Daly M S and Warburton R J 1994 *Physica* B **201** 271–9
[5] Wu X and Ulloa S E 1993 *Phys. Rev.* B **48** 144 407–15
[6] Sakaki H, Chang L L, Ludeke R, Chang C A, Sai-Halasz G A and Esaki L 1977 *Appl. Phys. Lett.* **31** 211–4
[7] Sai-Halasz G A, Tsu R and Esaki L 1977 *Appl. Phys. Lett.* **30** 651–8
[8] Sai-Halasz G A, Chang L L, Welter J M, Chang C A and Esaki L 1978 *Solid State Commun.* **25** 935–40
[9] Chang L L, Kawai N J, Sai-Halasz G A, Ludeke R and Esaki L 1979 *Appl. Phys. Lett.* **35** 939–43
[10] Guldner V, Vieren J P, Voisin P, Voos M, Chang L L and Esaki L 1980 *Phys. Rev. Lett.* **45** 1719–23
[11] Maan J C, Gulder Y, Vieren J P, Voisin P, Voos M, Chang L L and Esaki L 1981 *Solid State Commun.* **39** 683–7
[12] Bastard G, Mendez E E, Chang L L and Esaki L 1982 *J. Vac. Sci. Technol.* **21** 531–9
[13] Mendez E E, Chang L L, Chang C A, Alexander L F and Esaki L 1984 *Surf. Sci.* **142** 215–22
[14] Mendez E E, Bastard G, Chang L L, Chang C A and Esaki L 1984 *Bull. Am. Phys. Soc.* **29** 471–8
[15] Olego D, Pinczuk A, Gossard A C and Wiegmann W 1982 *Phys. Rev.* B **25** 7867–71
[16] Jain J K and Allen P B 1985 *Phys. Rev.* B **32** 997–1004
[17] Tselis A C and Quinn J J 1983 *Phys. Rev.* B **29** 3318–35
[18] Bloss W L 1991 *Phys. Rev.* B **44** 1105–12
[19] Das Sarma S and Madhukar A 1981 *Phys. Rev.* B **23** 805–15
[20] Camley R E and Mills D L 1984 *Phys. Rev.* B **29** 1695–706
[21] Zhu X, Xia X, Quinn J J and Hawrylak P 1988 *Phys. Rev.* B **38** 5617–23
[22] Sharma A C 1991 *Mod. Phys. Lett.* B **5** 455–63

[23] Hawrylak P, Wu J and Quinn J J 1985 *Phys. Rev.* B **32** 5169–76
[24] Katayama S and Ando T 1985 *J. Phys. Soc. Japan.* **54** 1615–26
[25] Tzoar N and Zhang C 1986 *Phys. Rev.* B **34** 1050–6
[26] Sood A K 1989 *Defence Sci. J.* **39** 411–23
[27] Sood A K, Menendez J, Cardona M and Ploog K 1985 *Phys. Rev. Lett.* **54** 2115–8
[28] Lambin Ph, Vigneron J P and Lucas A A 1985 *Phys. Rev.* B **32** 8203–15
[29] Pokatilov E P and Beril S I 1983 *Phys. Status Solidi* b **188** 567–73
[30] Bechstadt F and Ederlein R 1985 *Phys. Status Solidi* b **131** 53–66
[31] Lambin Ph, Vigneron J P, Lucas A A, Thiry P A, Liehr M, Pireaux J J, Caudano R and Kuech T J 1986 *Phys. Rev. Lett.* **56** 1842–5
[32] Das Sarma S and Quinn J J 1982 *Phys. Rev.* B **25** 7603
[33] Xia X, Zhu X, Hawrylak P, Eliason G and Quinn J J 1992 *Trends Plasma Sci.* **1** 31–8
[34] Sharma A C and Sood A K 1994 *J. Phys.: Condens. Matter* **6** 1553–62
[35] Wagner J, Schmitz J, Fuchs F, Ralston J D and Koidl P 1995 *Phys. Rev.* B **51** 9786
[36] Wagner J, Schmitz J, Richards D, Ralston J D and Koidl P 1996 *Solid State Electron.* **40** 281–5
[37] Behr D, Wagner J, Schmitz J, Herres N, Ralston J D and Koidl P 1994 *Appl. Phys. Lett.* **65**
[38] Ilegems M 1985 *The Technology and Physics of Molecular Beam Epitaxy* ed E H C Parker (New York: Plenum) pp 83–142
[39] Kittel C 1987 *Introduction to Solid State Physics* (New York: Wiley) pp 338, 309